



# Experimental Study on Steel–Concrete Composite Twin I-Girder Bridges

Weiwei Lin, Ph.D., M.ASCE<sup>1</sup>; Heang Lam, Ph.D.<sup>2</sup>; and Teruhiko Yoda, Ph.D., M.ASCE<sup>3</sup>

**Abstract:** A large number of steel–concrete composite twin I-girder bridges have been built in both Europe and Japan, but the lack of redundancy has always been a concern in the US and many other countries. In addition, very few experimental studies have been performed on mechanical performance of such bridges, particularly for the intact twin I-girder bridges. On this background, a steel–concrete composite twin I-girder bridge specimen was designed according to the current highway bridge design specification in Japan. Static loading tests were performed, and two loading conditions including both symmetric loading and asymmetric loading were applied. The load versus deflection relationship and strain development on the steel main girders and concrete slab at key sections were measured. The flexural strains on the lateral beam were also measured and reported in this paper to confirm the load transfer between two main girders. In addition, the shear strain of shear connectors (stud, in this study) was also measured to investigate the shear force transmission on the steel–concrete interface. The theoretical values were also provided to compare with the test results from the twin girder specimen under symmetric loading condition. The experimental results indicate that the theoretical analysis can predict the behavior of the twin girders very well in the elastic stage by considering the effective width of the slab. The performances of each structural component and load transfer path in such bridges were also discussed. DOI: [10.1061/\(ASCE\)BE.1943-5592.0001509](https://doi.org/10.1061/(ASCE)BE.1943-5592.0001509). © 2019 American Society of Civil Engineers.

**Author keywords:** Twin girder bridges; Steel–concrete composite; Experimental study; Theoretical analysis; Intact case.

## Introduction

Fig. 1(a), Multigirder bridges, as shown in are one of the most common types of medium-span composite bridge, which can be used for a single span or for continuous multiple spans, and it is particularly effective where construction depth is limited. In multigirder bridges, a number of similarly sized longitudinal plate girders are arranged at uniform spacing across the width of the bridge. The deck slab spans transversely between the longitudinal girders and cantilevers transversely outside the outer girders (Sarraf et al. 2013). The girders are braced together at supports and at some intermediate positions. Composite action between the reinforced concrete deck slab and the longitudinal girders is achieved by means of shear connectors welded on the top flanges of the steel girders. Because twin girder bridges are classified as nonredundant structures according AASHTO (2012) specifications, their construction was rather limited in the US and many other countries. Recently, however, the two-girder steel–concrete composite bridges have been widely used in practice in several other countries, like Japan. In comparison with traditional multigirder bridges, twin girder composite bridges have the following characteristics: the use of prestressed deck and composite deck makes the larger space between the main girders possible; the resistance of the deck for

the transverse load makes the omission of the lateral bracing possible; and fewer main girders and lateral beams make simplification of the bridge design and significant reduction of the construction cost possible.

Twin girder bridges have been widely built in Europe, such as the Rudolf von Habsburg Bridge (1971) in Germany, Jassans-Riottier Bridge (1971), Monestier Viaduct, and the Triel-sur-Seine Bridge in France, whose main spans are longer than 100 m. In Japan, the application of twin girder bridges is of historical inevitability. In the Showa period (1926–1989), due to the lack of construction materials (particularly structural steel) and their high cost, complex design of multigirder bridges was popular because the structural steel can be efficiently used and saved. During the Heisei period (1989–present), however, the situation changed. With the significant reduction of the number of highly skilled workers, the long construction time and high labor cost involved in building multigirder bridges became a severe problem (Inaba 2011). On the contrary, the material cost increased little in comparison with the labor cost. It is in this context that minority main girder bridges with simple sections became in demand. In 1992, a trial bridge (Shinkotoni viaduct) was built in Hokkaido, and the construction cost was greatly reduced by using two main girders with fewer cross bracings and a standardized connecting plate. The research achievements were provided in “Design Guidelines for Steel Highway Bridges (Draft),” (Ministry of Construction 1995) and bridges with fewer main girders were recommended for practical use and called rationalized girder bridges thereafter. In 1995, another twin girder bridge (the Horonai River Bridge) was built in Hokkaido. The girder distance was extended from the often used value of 2–3 m to around 6 m by using prestress in the concrete slab. Thereafter, more and more twin girder bridges were built in the Japanese highway system, including the Warashinagawa Bridge (awarded the Japan Society of Civil Engineers Tanaka Prize in 2007), which has two main girders with girder distance of nearly 10 m.

<sup>1</sup>Associate Professor, Dept. of Civil Engineering, Aalto Univ., 02150 Espoo, Finland (corresponding author). Email: [weiwei.lin@aalto.fi](mailto:weiwei.lin@aalto.fi)

<sup>2</sup>Structural Engineer, TTH Construction, 12158 Phnom Penh, Cambodia. ORCID: <https://orcid.org/0000-0002-0418-7453>. Email: [lamheang@aoni.waseda.jp](mailto:lamheang@aoni.waseda.jp)

<sup>3</sup>Emeritus Professor, Dept. of Civil and Environmental Engineering, Waseda Univ., Shinjuku-ku, Tokyo 169-8555, Japan. Email: [yoda1914@waseda.jp](mailto:yoda1914@waseda.jp)

Note. This manuscript was submitted on July 24, 2018; approved on July 29, 2019; published online on October 25, 2019. Discussion period open until March 25, 2020; separate discussions must be submitted for individual papers. This paper is part of the *Journal of Bridge Engineering*, © ASCE, ISSN 1084-0702.

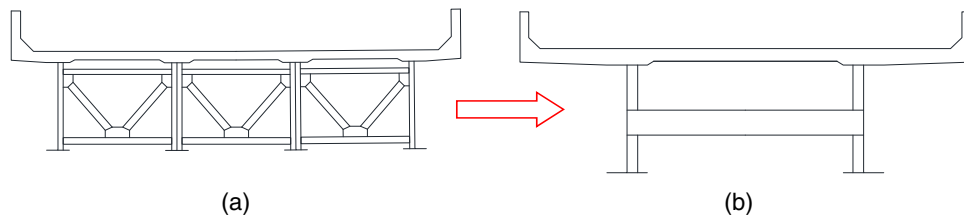


**Fig. 1.** Traditional multi-girder composite section and new structural form of twin girder composite section: (a) multi-girder composite section; and (b) twin girder composite section.

Recent studies on two-girder bridges mainly focused on the postfracture redundancy and redundancy evaluation of twin girder systems, such as those performed by Idriss et al. (1995), Tachibana et al. (2000), Park et al. (2012), Samaras et al. (2012), Kim and Williamson (2015), and Lin et al. (2013, 2016). Limited studies on intact twin girder bridges were also performed, mainly focusing on connection details such as the diaphragm, buckling of main girders, and shear lag effect in slabs. Takahashi et al. (1997) performed an experimental study to investigate the structural details of the connection of the diaphragm used in the first steel twin girder bridge, the Horonai River Bridge. Four types of connection details, including the connection with the triangular rib plate or connection plate, split-tee connection, and endplate connection, were investigated. Hotta et al. (1999) investigated both global and local lateral-torsional buckling of twin girder bridges during erection of main girders in the case of the incremental launching method. Dezi et al. (2006) performed an analysis to investigate the shear lag effect in slabs of twin girder steel-concrete composite decks due to the main prestressing techniques such as support settlements, bonded cables inside the concrete slab, and external slipping tendons. Kozy and Tunstall (2007) reported stability analysis results of a twin I-girder pedestrian bridge constructed in Minnesota, and they pointed out that the strength of noncomposite twin girder systems without lateral bracing can be controlled by the limit state of system or global buckling. Awall and Hayashikawa (2011) performed a parametric study on horizontally curved twin I-girder bridges, focusing on the effects of curvature on the impact factor of such bridges. Ma and Shi (2016) performed numerical analysis to investigate the parameters that affect the stability and capacities on twin I-girder systems. Parameters considered in this study include girder depths, flange width to thickness ratio, web depth to thickness ratio, number of stiffeners, and cross-beam spacing. However, an experimental study on the mechanical behavior of intact twin I-girder bridges was rarely performed. In order to promote the application of such bridges, fundamental studies on such structures become necessary.

Based on this background, studies on the mechanical behavior of twin girder bridges were conducted. The experimental studies of twin I-girder bridges were divided into two parts: intact case and damaged case. In the intact case, the mechanical behavior of twin I-girder bridges under normal service conditions was investigated to understand the serviceability, ductility, and safety of such bridges. For the damaged case, the mechanical behavior of such bridges under extreme conditions (e.g., member fracture) was investigated, focusing on the structural redundancy and resilience. The experimental results of the intact specimen are reported in this paper.

## Experimental Program

### Test Specimen

A simply supported steel-concrete composite twin I-girder bridge specimen was designed according to Japanese bridge design

specifications (JRA 2012; JSCE 2007). The specimen was designed as 4.4 m in length and was simply supported at a span length of 4 m by considering the available space in the structural laboratory. The width-to-span ratio and depth-to-width ratio were taken to be similar to that of typical composite twin I-girder bridges used in Japan. Two I-girders with a height of 300 mm were used as main girders, and the width of the concrete slab was determined as 1,200 mm. According to bridge design specification in Japan (JRA 2012), the minimum thickness of a concrete slab is 110 mm. To also study the real behavior of studs and avoid possible damage to the slab during transportation, the slab thickness was determined as 120 mm. The influence of the deck thickness on general behavior of such structures was investigated based on numerical analysis (Lam 2017; Lam et al. 2017), and the results clearly indicate that the thickness of the concrete slab as well as the concrete strength have no effect on the global behavior of such structures. Vertical stiffeners were welded at support points and other key sections at an interval of 400 mm to prevent buckling failure and crippling of the web before flexural failure. Six cross beams (CB-1 to CB-6) were also used between the twin main girders for load redistribution. Vertical stiffeners on the web were also appropriately designed and arranged between cross beams. Four rows of shear stud connectors with the diameter of 16 mm were placed with a uniform spacing of 200 mm in the longitudinal direction to ensure the full (or complete) connection between the steel girder and the concrete slab. The theoretical values of yield and ultimate bending moment capacity of the specimen considering the actual yield stress from the material tests were determined as 676 and 886 kN · m, respectively. Size dimensions and design details of the test specimen are shown in Fig. 2.

### Instrumentation

The instrumentation of the loading test is shown in Fig. 3. LVDTs were used to measure the vertical deformation at the span center section and support location at both ends. With the purpose of determining the neutral axis, strain gauges were used to measure the strain in the web, steel flanges, and the reinforcement as well as the concrete slab surface in key sections. In addition, shear strain on stud connectors in both longitudinal and lateral directions were also measured.

### Test Setup and Loading Procedure

A testing machine with a loading capacity of 5,000 kN was used to apply the load in the test. The test specimen was supported by a roller system at two ends. Two loading conditions were used in this study. In the first stage, a concentrated load was applied symmetrically by placing a loading beam on the top of the concrete slab in the midspan section, as shown in Fig. 4(a). Three loading plates in total were used. Two were used between the loading beam and the concrete slab, located right above the main girders, and the third loading plate was used on the middle of the loading beam. In this

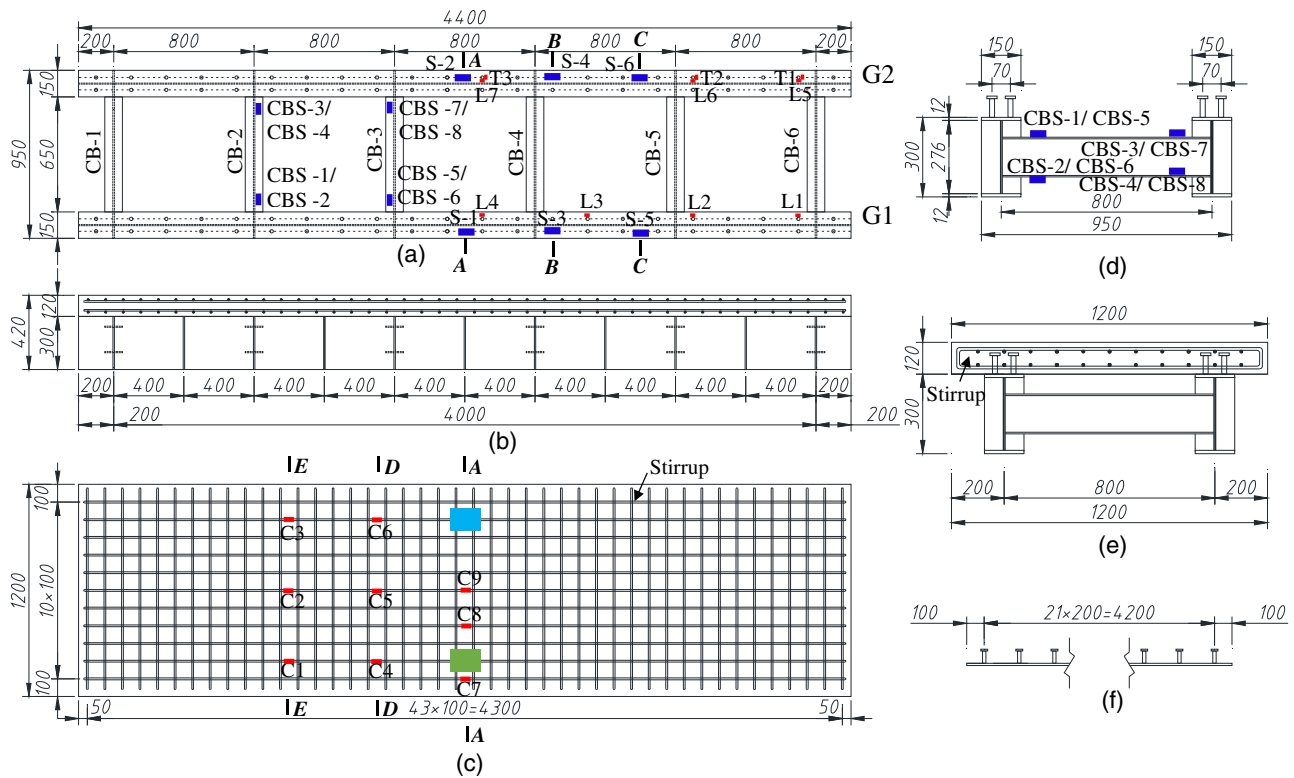


**Fig. 2.** Size dimensions of the connection joint after strengthening (unit: millimeters): (a) plane view of steel girder and shear strain gauge on studs; (b) side elevation; (c) plane view of concrete deck and reinforcement; (d) cross-section of steel girder; (e) composite section; and (f) stud distribution.

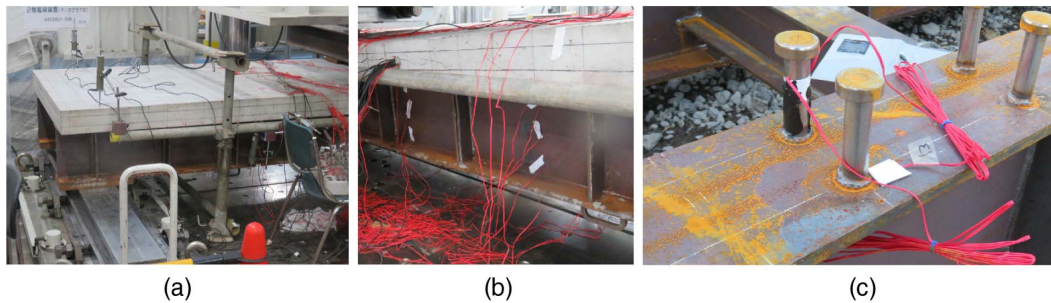


**Fig. 3.** Instrumentation in the loading test: (a) LVDT for displacement; (b) strain gauges on main girder; and (c) strain gauges on stud.

stage, the applied load was controlled to be less than 150 kN (about 22% of the yield load of the twin girder) to avoid any possible damage of the test specimen. In the second stage, the load was applied asymmetrically right on top of one main girder (G1), as shown in

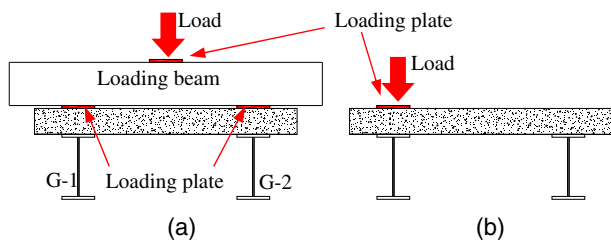


**Fig. 4.** Loading conditions: (a) symmetric load; and (b) asymmetric load.

Fig. 4(b). The load was applied by static loading with unloading process. The loading was terminated when either the maximum stroke of the jack was reached or the load level of the test specimen dropped significantly. In both symmetrical and asymmetrical loading conditions, preloading until 50 kN was applied to check the reliability of the measuring equipment and the stability of the test specimens. The displacement control method was used in the loading process with loading rates of 0.004 mm/s for the preloading and 0.008 mm/s for following loading test. The test specimen was supported by a roller system at two ends. The setup of the specimen in the experiment is shown in Fig. 5.

### Material Properties

Concrete cylinders of 10 cm (diameter) × 20 cm (height) were prepared for compressive tests during casting of the concrete slab. The concrete compressive strengths achieved after 28 days of curing were 28.8, 29.5, and 29.5 MPa, respectively, with the average



(a)



(b)

**Fig. 5.** Loading test setup: (a) symmetric load ( $P < 150$  kN); and (b) asymmetric load.

compressive strength of 29.3 MPa. The structural steel of SM490 was used for the steel girder in this specimen. The web had a thickness of 6 mm, and both top and bottom flanges had a thickness of 12 mm. According to the tensile test results, the yield strength and ultimate strength of the structural steel for web were 450 and 577 MPa, respectively, while the yield strength and ultimate strength of structural steel for top and bottom flanges were 389 and 548 MPa, respectively. The reinforcement of the D10 nominal diameter was used for both longitudinal reinforcement and stirrup reinforcing bars in the concrete slab. According to the test results, the yield strength and ultimate strength of the reinforcement were 406 and 544 MPa, respectively. The stud shear connectors were

made of SS400, which has a nominal yield strength of 235 MPa and an ultimate tensile strength of 400 MPa, respectively.

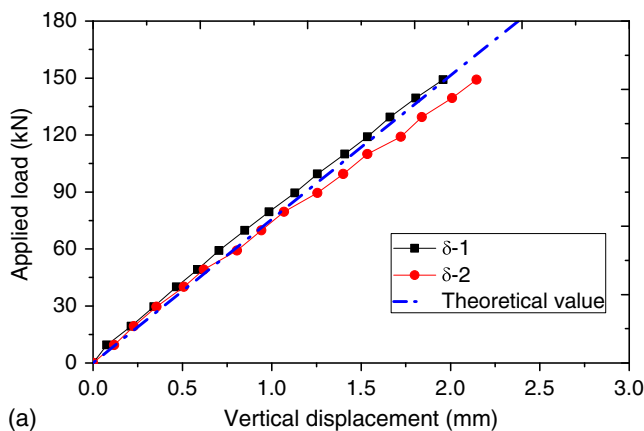
## Test Results and Discussion

### Load–Deflection Response

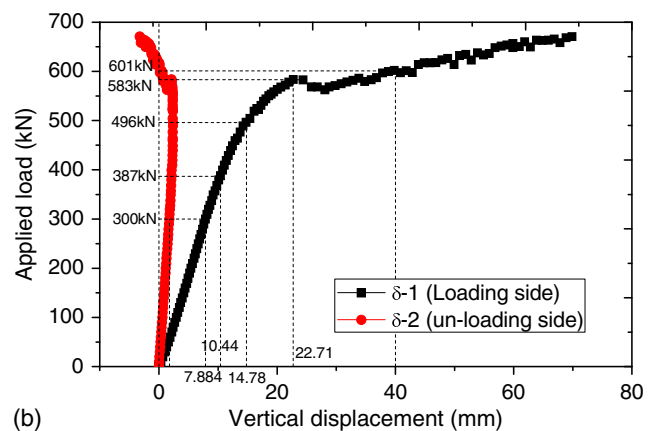
The load–vertical displacement curves of the test specimen under both symmetrical and asymmetrical loading are illustrated in Fig. 6. The displacement was taken at the midspan section of the test specimen. Due to space limitations under the deck, the LVDTs were used on the bottom of the concrete slab but not the bottom of the main girders. The displacements on Girder 1 (G1) and Girder 2 (G2) are referred to as  $\delta-1$  and  $\delta-2$ , respectively. For asymmetrical loading, the load was only applied on G1, as shown in Fig. 4.

When subjected to a symmetrical load, the load–vertical displacement curves are shown in Fig. 6(a). It can be found that both  $\delta-1$  and  $\delta-2$  increase linearly with the increase of the applied load. Though there is a small difference, the displacement of  $\delta-1$  was similar to that of  $\delta-2$ , indicating that identical loads were applied on the two main girders. In addition, the theoretical value of the load–displacement curve of the specimen was also provided. In computing the theoretical value, all the materials were assumed to be elastic and the effective width of the concrete slab was considered to account for the shear lag effects. The effective width of the concrete slab in twin I-girder bridges was determined according to Eq. (1) according to the “Specifications for Highway Bridges” (JRA 2012) in Japan. Full connection was assumed for the steel–concrete interface, and the transformed section method was used to determine the moment of inertia of the composite section. The theoretical values were then determined according to the classic theory for simply supported girders. The comparison indicates that the theoretical results determined according to current elastic design theory agree well with the test results, demonstrating the twin I-girder bridges can be designed appropriately on the basis of the current bridge design method

$$\lambda = \begin{cases} b & \left( \left( \frac{b}{l} \right) \leq 0.05 \right) \\ \left\{ 1.1 - 2 \left( \frac{b}{l} \right) \right\} b & \left( 0.05 < \left( \frac{b}{l} \right) < 0.30 \right) \\ 0.15l & \left( 0.30 \leq \frac{b}{l} \right) \end{cases} \quad (1)$$



(a)



(b)

**Fig. 6.** Load–displacement relationships: (a) symmetric load ( $P < 150$  kN); and (b) asymmetric load.

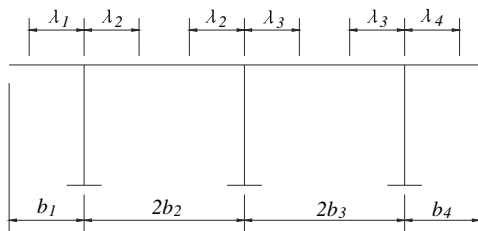


Fig. 7. Effective width of flange.

where  $\lambda$  = half effective width of flange (mm);  $b$  = half spacing between webs or projection width of cantilever portion (mm) (Fig. 7); and  $l$  = equivalent span length (mm).

When subjected to an asymmetric load, the load–vertical displacement relationships are shown in Fig. 6(b). In the initial loading stage, both  $\delta$ -1 and  $\delta$ -2 increase linearly with the load increases. However,  $\delta$ -1 was much larger than  $\delta$ -2, caused by the asymmetrical load applied on the side of G1. Taking the applied load of 300 kN as an example, the corresponding displacement at G1 (7.884 mm) was nearly 4.5 times the displacement at G2 (1.764 mm), thus G2 carries around 18.3% [= 1.764/(1.764 + 7.884)] of the load carried by the main girders. The results indicate that before crush or cracking, the concrete slab is capable of transferring a certain level of applied load from G1 to G2, but not zero as can be predicted according to the lever principle.

When the load increases to  $P = 387$  kN, the yielding was confirmed on the web–bottom flange junction of G1. Thereafter,  $\delta$ -1 increased much faster, while  $\delta$ -2 increased much slower with the increasing load. Even so,  $\delta$ -2 kept increasing before it started to decrease when the load reached 496 kN. When the load increased beyond 496 kN,  $\delta$ -1 kept increasing remarkably, while  $\delta$ -2 kept decreasing and remained in the elastic stage. This phenomenon clearly indicates that G2 carries little load after the yielding of G1, and the applied load was mainly sustained by G1 and the concrete deck.

When the applied load increased to 583 kN, a sudden drop of the applied load was observed due to the local failure of the concrete slab at the loading position. With the increase of the displacement (displacement control method was used in the loading test), the applied load increased again, reflecting the rebalance at the loading point. Thereafter, turnover behavior of the test specimen started to occur, which can be indicated from the sharp increase of  $\delta$ -1 and decrease (or reverse increase to upward direction) of  $\delta$ -2. Thereafter,  $\delta$ -1 kept increasing quickly with the increase of the load,

while the downward displacement of  $\delta$ -2 kept decreasing and then began the upward displacement. In this stage, the load carried by G1 had been increasing, while the load carried by G2 had been decreasing due to the damage of the concrete slab and insufficient load transfer or redistribution capacity of the cross beams and damaged concrete deck.

In general, the functional limit state of a structure can be determined as the maximum vertical deflection of the superstructure reaching a value equal to the span length divided by 100 (40 mm for the specimen used in this study) (Lin et al. 2013). In this study, however, vertical displacement of G1 had been loaded to nearly 70 mm and no sudden failure was observed. In this study, the failure mode of the specimen can be concluded as the local failure of the concrete slab at the loading point due to concrete crushing, the cracking (top surface) and the stripping of the concrete slab (bottom surface) due to the torsion, and lateral bending (bending moment perpendicular to the bridge axis) caused by the eccentric loading, as shown in Fig. 8.

### Strain on the Steel Main Girders

Six strain gauges were attached on the bottom flange of the steel girder on three key sections (Section A, Section B, and Section C), denoted by S-1 to S-6, as shown in Fig. 2(a). The strain results of the steel bottom flange under both symmetric and asymmetric loadings were measured in the tests and illustrated.

When the specimen was subjected to symmetric loading, the strain on the steel girder was as shown in Fig. 9. The corresponding theoretical relationships between the applied load and the strain on the basis of the elastic theory at Section A, Section B, and Section C (denoted as Theoretical value-A, Theoretical value-B, and Theoretical value-C, respectively) are also provided. Both strains on G1 and G2 increase linearly with the increase of the load, and the strains on G1 were similar to those on G2. Also, the comparison shows that the theoretical results agree well with the measured results in all three sections, indicating the applicability of elastic design theory in designing such bridges.

When the specimen was subjected to asymmetric loading, the strain on the bottom flange of the steel girder in the midspan section was as shown in Fig. 10. In the initial loading stage, both strains on G1 and G2 increased linearly as the load increased, as shown in Fig. 10(b). However, the strain on G1 was much larger than that on G2, which was due to the different vertical displacement as discussed in the previous section. Taking the applied load of 300 kN as an example, the corresponding strain on G1 (1,184 microstrains) was nearly 2.75 times of that on G2, indicating that G1 carries



Fig. 8. Failure mode of the test specimen: (a) top view; and (b) bottom view of the concrete slab.

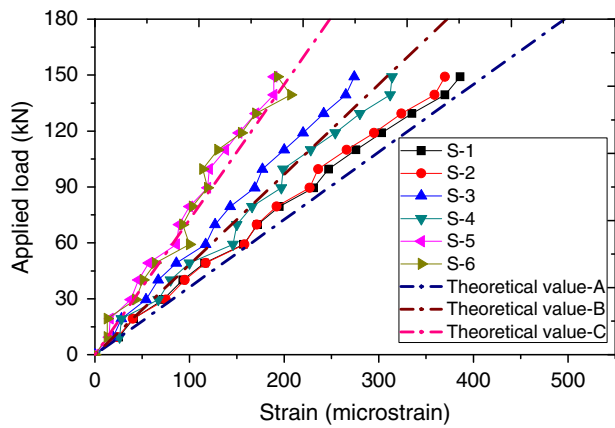


Fig. 9. Strain on bottom flange (symmetric load).

nearly 73% of the load on the main girders. In the plastic stage ( $P \geq 387$  kN), however, this ratio becomes smaller and smaller with the load increase. Due to the local crush and cracking of the concrete slab, the load transmission capacity between two main girders becomes less and less. Different from the displacement reduction confirmed in Fig. 6(b), strain reduction on G2 was not confirmed. This is presumably because of the torsional deformation of the girder caused by the eccentric loading.

When the load reached the peak load (670 kN), because strain on the bottom flange of G1 was already around 45,000 microstrains, it can be considered as the ultimate state of the composite girder. However, the corresponding maximum strain on G2 was only

1,618  $\mu$ , indicating that the unloaded girder (G2) was still in the elastic stage. Therefore, the load transformation between two main girders in the plastic stage was relatively small.

### Strain on Concrete Slab

Nine strain gauges were installed on the top surface of the concrete slab on three key sections (Section A, Section D, and Section E), denoted by C1–C9, as shown in Fig. 2(c). For Section D and Section E, two strain gauges were employed on the right top of the steel girder, and the other one was used in the middle between them. For Section A, two strain gauges were used on the two sides of a loading plate, and the third gauge was used on middle of the concrete slab. The detailed locations of the strain gauges are shown in Fig. 2. The strain results of the concrete under both symmetric and asymmetric loadings were measured in the tests and are shown in Figs. 11 and 12, respectively.

When two symmetric loads were applied, the normal strain on the top surface of the concrete slab was as shown in Fig. 11. The corresponding theoretical values of the normal strain according to elastic theory were also determined and are provided. The results indicate that the normal strain on the concrete increased linearly with the increase of the applied load. For Sections A and B, the normal strains on the right top of the main girders (C1, C3, C4, and C6) are close to the strain on the middle top of the cross section (C2 and C5), indicating the negligible shear lag effect of the concrete slab under symmetric loads. This is also confirmed the effective width calculation for the concrete slab. According to Eq. (1), the effective width of the concrete slab is determined to be 1.12 m, which is very close to the actual width of the slab

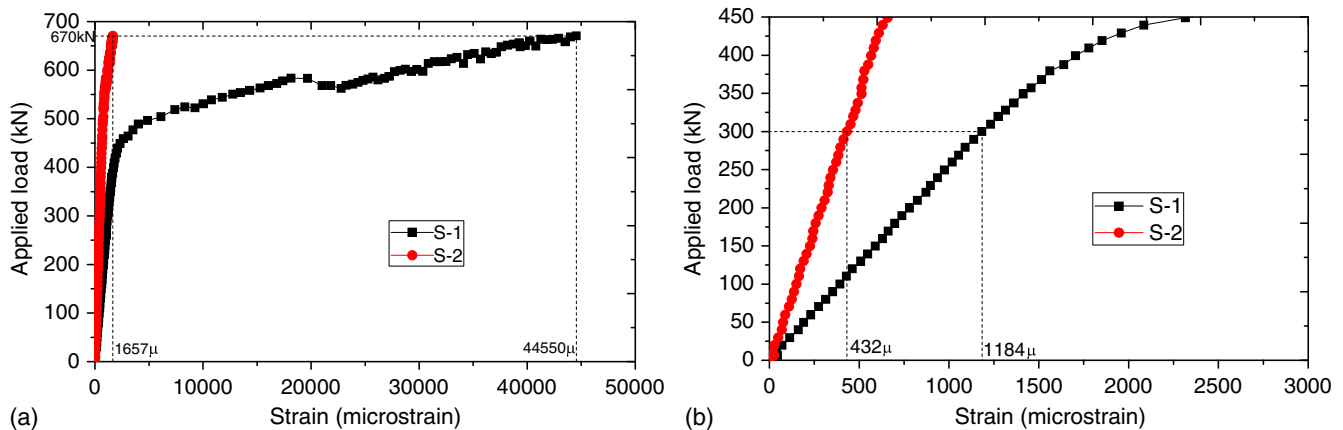


Fig. 10. Strain on bottom flange (asymmetric load): (a) whole loading stage; and (b) initial loading stage.

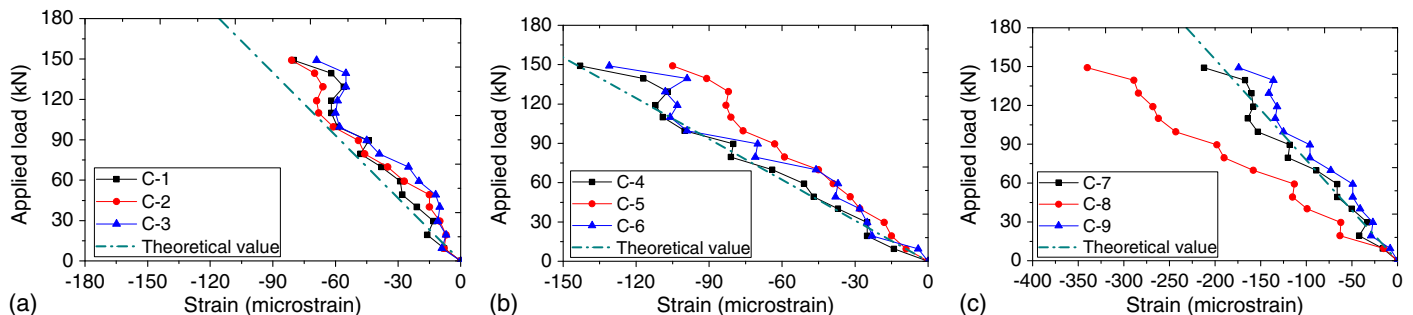
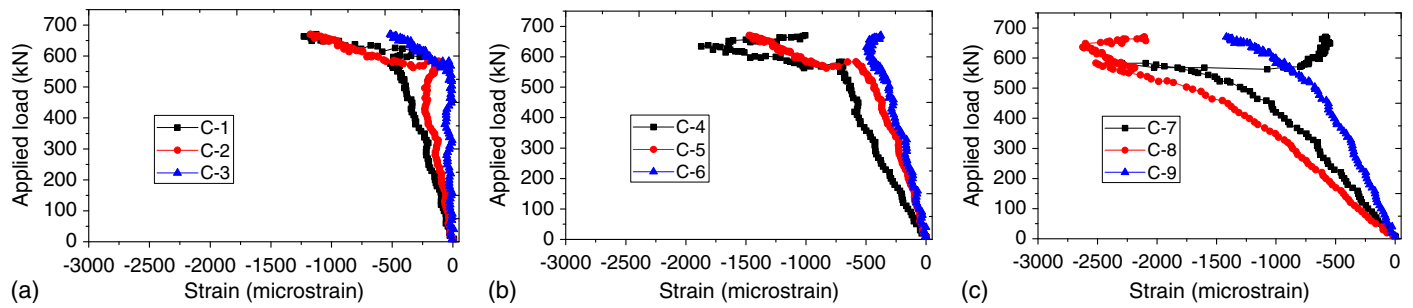


Fig. 11. Normal strain on top surface of the concrete slab (symmetric load): (a) Section A; (b) Section D; and (c) Section E.



**Fig. 12.** Normal strain on top surface of the concrete slab (asymmetric load): (a) Section A; (b) Section D; and (c) Section E.

(1.2 m). Also, the comparison shows that the theoretical results agree well with the measured results in all three sections, indicating the applicability of elastic design theory in designing such bridges.

When the applied load changes to asymmetric loading, the strain on the top surface of the concrete slab at all measured sections (Section A, Section D, and Section E) was as shown in Fig. 12. In the initial loading stage ( $P \leq 300$  kN), normal strains on all three sections increased linearly as the load increases, as shown in Fig. 12(b). After that, the strain kept increasing until the load increased to 583 kN, when the local failure of the concrete slab and sudden drop of the applied load was observed. As a result, decreasing of the normal strain was observed at C1, C4, C7, and C8. The strain at C1 and C4 kept decreasing even after the rebound of the applied load, indicating the local failure of at the loading point. Also, as the normal strains of C7 and C8 were still smaller than the ultimate strain of concrete [ $-3,500 \mu$  according to JSCE (2012)], the failure of the concrete was due to the combined effects of the vertical compression and longitudinal compression caused by the applied load and bending moment. For strain gauges at other locations of the concrete slab, the strain of the concrete kept increasing with the increase of the applied load, indicating that the concrete slab remains effective in carrying and distributing the applied load to a certain extent until the ultimate load.

### Strain on Cross Beams

Cross beams are important members in multi-main-girder bridges to prevent the buckling of the main girders and for load redistribution between main girders (Lin et al. 2019). In twin girder bridges, however, the effectiveness of cross beams is not clear, and their behavior is still not well defined. Because of the unclear behavior of cross beams in twin girder bridges, twin girder bridges are generally considered as nonredundant. In this study, eight flexural

strain gauges (CBS-1 to CBS-8) were attached to the two cross beams (CB-2 and CB-3), as shown in Fig. 2(a). Strain gauges were attached on both top and bottom at the end sections.

The load–flexural strain results of two cross beams are shown in Fig. 13. As the flexural strain keeps increasing with the increase of the load, the cross beams in twin girder bridges are functional. Also, it was found that the further the cross beam was located from the loading point, the larger the strain that can be confirmed. The deformation of cross beams may consist of vertical deformation, longitudinal deformation, and twist deformation. Because the vertical deformation decreases with the distance from the cross beams to loading point, the strain was mainly caused by the lateral deformation of the beam. Another interesting phenomenon is that the flexural strain on both top and bottom flanges in cross beams have the same sign conversion, indicating that they are in either tension or compression simultaneously. If the cross beams are mainly subjected to vertical forces (shear or bending), the flexural strain on top and bottom flanges should have equal (or similar) strain values with different sign conversion. When subjected to asymmetrical loading, however, lateral bending (bending moment perpendicular to the cross-beam axis) and the torsional moment will occur in cross beams due to the relative deformation between the two main girders, which might be the major cause for this phenomenon. This is not going to happen if the cross beams are mainly subjected to vertical bending. Therefore, in comparison with the load-carrying capacity for vertical bending, the cross beams are more functional for sustaining the lateral bending (bending moment perpendicular to the cross-beam axis) and the torsional moment.

### Strain Results on Shear Connectors

Although existing research provided preliminary information on the behavior of shear connectors in composite structures, most

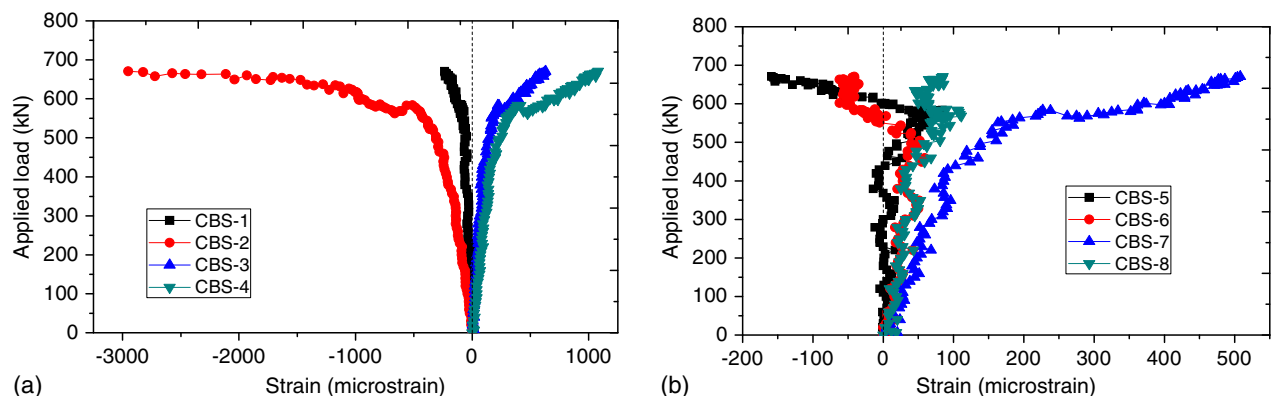


**Fig. 13.** Normal strain on cross beams: (a) CB-2; and (b) CB-3.

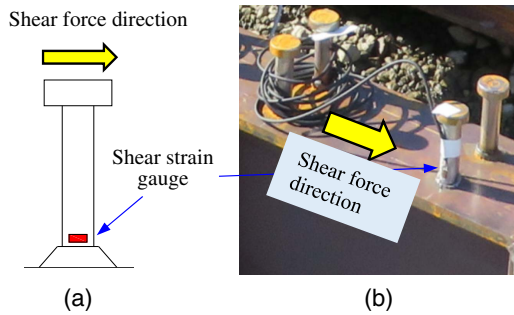


**Fig. 14.** Shear strain gauge on shear stud: (a) shear strain gauge location; and (b) stud in the test specimen.

studies were generated and analyzed from push-out tests. The specimens were short and had a limited number of shear connectors, and the tests were essentially pure shear tests (Yen et al. 1997). Also, flexural strain was mostly measured instead of shear strain, in view of studies performed by Lin et al. (2014). In actual twin I-girder structures, the composite girder is subjected to bending moment and transverse shear forces, and the specimens contain many more shear connectors. Based on this background, the shear strain at the foot of the studs was measured in the loading tests, as shown in Fig. 14. There were 10 shear strain gauges in the test specimen, as shown in Fig. 2(a). Shear strain gauges L1–L4 were used to measure the shear strain of studs in longitudinal direction on G1, while L5–L7 were used to measure that of studs on G2. Also, in order to confirm the shear strain of a stud in the transverse direction, another three strain gauges (T1–T3) were attached on studs in G2.

Shear strain results of studs in the loading tests subjected to symmetric load are shown in Fig. 15. Also, the theoretical prediction of the longitudinal shear strain at the measured location based on elastic theory is provided. Complete connection was assumed on the steel–concrete interface, which means the slip on the interface was not considered. The theoretical value of longitudinal shear strain was determined by using the following equation:

$$\gamma = \frac{VQ}{GI t} \quad (2)$$

where  $\gamma$  = shear strain at foot of the stud;  $V$  = shear force;  $G$  = shear modulus of the stud;  $I$  = second moment of cross-sectional area (twin I-girder section considering effective width of the concrete slab);  $t$  = actual width of the section at the position where  $\gamma$  is being calculated (total width of top flanges of the twin girder in this study); and  $Q = A'\bar{y}$ , where  $A'$  is the area of the top portion of

the cross-sectional area above the measured location, and  $\bar{y}$  is the distance from the neutral axis to the centroid of  $A'$ .

The longitudinal shear strain of studs on G1 and G2 are shown in Fig. 15. A zigzag increase of shear strain on studs was observed, which might be caused by shear force transmission at the initial loading stage. Theoretically speaking, the shear strain at different sections should be the same due to the same shear forces under symmetric loading applied at the midspan. However, the strain results in Figs. 15(a and b) indicate that the shear strain on studs near the quarter-span was larger than those on studs near the girder end section or midspan section, which was similar to the results observed in previous tests (Lin et al. 2014), and the fraction forces on the interface caused by reaction forces at the supports and the applied loads are considered as the main reasons. In addition, the comparison indicates that the theoretical results agree well with the results of the measured shear strain at L1 and L2, but slightly larger than the results at L3 and L4. Therefore, it can be confirmed that the slip on the steel–concrete interface can be ignored at the elastic stage, and full shear connection can be used for designing the twin I-girder bridges with full connection. On the other hand, the results in Fig. 15(c) indicate that the shear strain of studs in the lateral direction has a similar increasing trend as that in the longitudinal direction as shown in Figs. 15(a and b).

When subjected to an asymmetric load, the shear strain increase on studs versus applied load relationship was as shown in Fig. 16. The results in Fig. 16(a) show that shear strains on all measured studs increased linearly with increase of the applied load at the linear stage. After that, shear strains increased significantly as the applied load increased, which might be caused by two reasons: upward movement of the neutral axis and breaking of the bonding on the interface. After the yielding of the bottom flange, the neutral axis on G1 moved from the elastic neutral axis (in the web of the steel girder) to the steel–concrete interface, which caused the higher shear force transmission on the interface. On the other hand, the failure of the chemical bond or friction on the steel–concrete interface caused the shear force transmission from the chemical bond to the stud shear connectors. In addition, the comparison of the shear strain on different studs on G1 indicates a similar conclusion as that observed in Fig. 15, that the maximum shear strain is more likely to occur on studs near the quarter-span. Approximately equal shear strain according to the constant shear force distribution was not confirmed at the measured studs on G1. The shear strains on studs near the girder end and near the midspan are likely to be smaller, which might be caused by the friction forces on the interface due to the reaction force and the applied load at the girder end and midspan, respectively. The shear strain shown in Fig. 16(a) indicates that the shear studs on G2 undertake very small shear force under the concrete crush, indicating that little shear force

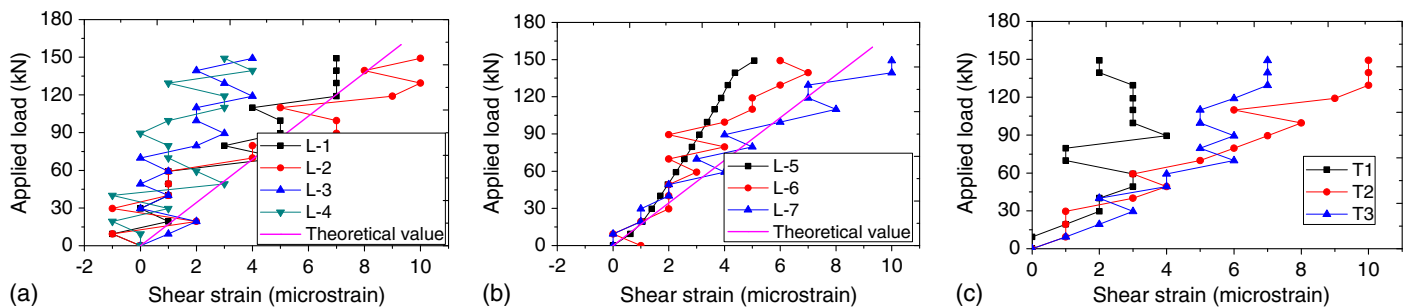


**Fig. 15.** Longitudinal and transverse shear strain on shear studs (symmetric load): (a) longitudinal shear strain, G1; (b) longitudinal shear strain, G2; and (c) transverse shear strain, G2.

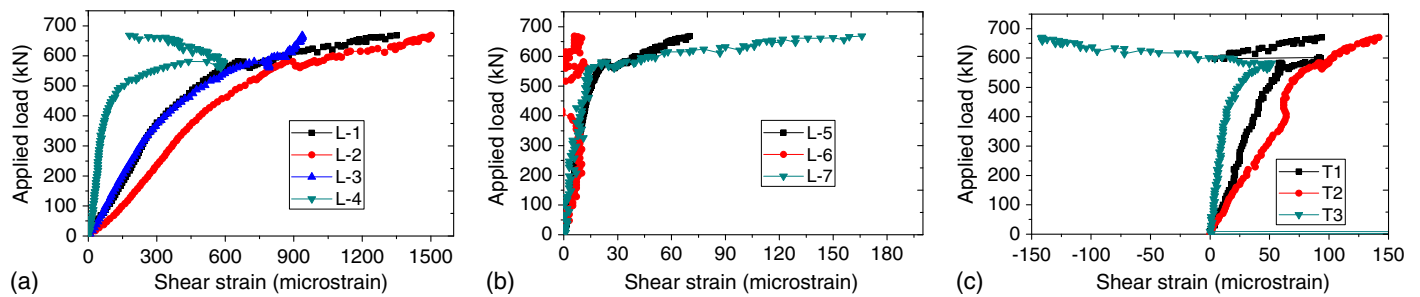


**Fig. 16.** Longitudinal and transverse shear strain on shear studs (asymmetric load): (a) longitudinal shear strain, G1; (b) longitudinal shear strain, G2; and (c) transverse shear strain, G2.

was transmitted from G1 to G2. When the applied load increased to 583 kN (local crush of concrete), significant shear strain increase was observed on L5 and L7, but little increase was observed in L6. However, all the shear strains are relatively smaller than those observed in studs on G1. It can be concluded that for an asymmetric load applied right top of the one main girder, the shear force transmission on the other main girder (unloaded girder) can be ignored. Fig. 16(c) shows the transverse shear strain at the foot of studs on G2. It can be seen that the transverse shear strain of shear studs on G2 was much larger than their longitudinal shear strains in both the elastic and plastic stages. Therefore, the results clearly indicate that the combination of shear strains at both longitudinal and transverse directions should be considered in the design of studs in twin I-girder steel–concrete composite bridges.

## Concluding Remarks

Static loading tests were performed on an intact steel–concrete composite twin girder bridge model. Detailed static loading tests involving load–displacement response and load–strain relationships on the steel girder, concrete slab, stud shear connectors, and cross beams were reported and examined carefully in this paper. Two loading conditions including both symmetrical loading and asymmetrical loading were applied in the loading test. From the results presented herein, the following conclusions and recommendations are made:

- The theoretical results determined according to the current elastic design theory, including both displacements on different sections and strains on different members, agree well with the test results. Therefore, twin I-girder bridges can be designed appropriately according to the current bridge design method.
- The unloaded girder needs to carry a certain amount of load applied on the right top of the other main girder in the elastic stage. The concrete slab is the key member in load transmission and distribution between two main girders. The load distribution capacity of the deck decreases significantly after concrete failure.
- Failure of the steel–concrete twin I-girder bridges is governed by the concrete crush. Under asymmetric loading, the failure mode of the specimen was due to the local failure of the concrete slab at the loading point due to crush, the cracking on the top surface, and the stripping on the bottom surface of the concrete slab due to induced torsion and lateral bending.
- Cross beams in the twin girder bridges are functional in load transmission and deformation compatibility between the two main girders. Cross beams contribute more to constraining the longitudinal and torsion deformation than redistributing the vertical load between the two main girders.
- In twin girder bridges, the combination of shear strain at both longitudinal and transverse directions in stud shear connectors

was confirmed in the loading test, and it should be considered in the design of studs in such bridges. Also, the maximum shear strain of stud shear connectors is more likely to occur on studs near the quarter-span.

## Data Availability Statement

Some or all data, models, or code generated or used during the study are available from the corresponding author by request.

## Acknowledgments

This research was sponsored by Waseda University Grant for Special Research Project-A (key funding, Project No.: 2015A-503; Grant Recipient: Weiwei Lin). The financial support is gratefully acknowledged.

## References

- AASHTO. 2012. *AASHTO LRFD bridge design specifications*. 6th ed. Washington, DC: AASHTO.
- Awall, M. R., and T. Hayashikawa. 2011. “Parametric study on dynamic interaction of horizontally curved twin I-girder bridges and a moving vehicle.” *J. Struct. Eng.* 57A: 242–251. <https://doi.org/10.11532/structcivil.57A.242>.
- Dezi, L., F. Gara, and G. Leoni. 2006. “Effective slab width in prestressed twin-girder composite decks.” *J. Struct. Eng.* 132 (9): 1358–1370. [https://doi.org/10.1061/\(ASCE\)0733-9445\(2006\)132:9\(1358\)](https://doi.org/10.1061/(ASCE)0733-9445(2006)132:9(1358)).
- Hotta, T., J. Naito, and N. Nishimura. 1999. “Lateral-torsional buckling strength of steel twin girder bridges under erection.” *J. Jpn. Soc. Civ. Eng.* 612 (46): 287–296. [https://doi.org/10.2208/jjscej.1999.612\\_287](https://doi.org/10.2208/jjscej.1999.612_287).
- Idriss, R. L., K. R. White, C. B. Woodward, and D. V. Jauregui. 1995. “After-fracture redundancy of two-girder bridge: Testing I-40 bridges over Rio Grande.” In *Proc., 4th Int. Bridge Engineering Conf.*, 316–326. Washington, DC: Transportation Research Board.
- Inaba, N. 2011. “Research on practical application of steel-concrete twin I-girder bridges.” [In Japanese.] Ph.D. thesis, Dept. of Civil and Environmental Engineering, Saitama Univ.
- JRA (Japan Road Association). 2012. *Specifications for highway bridges. Part I, Common Specification*. Tokyo: JRA.
- JSCE (Japan Society of Civil Engineers). 2007. *Standard specifications for steel and composite structures*. Tokyo: JSCE.
- JSCE (Japan Society of Civil Engineers). 2012. *Standard specifications for steel and composite structures*. Tokyo: JSCE.
- Kim, J., and E. B. Williamson. 2015. “Finite-element modeling of twin steel box-girder bridges for redundancy evaluation.” *J. Bridge Eng.* 20 (10): 04014106. [https://doi.org/10.1061/\(ASCE\)BE.1943-5592.0000706](https://doi.org/10.1061/(ASCE)BE.1943-5592.0000706).
- Kozy, B., and S. Tunstall. 2007. “Stability analysis and bracing for system buckling in twin I-girder bridges.” *Bridge Struct.* 3 (3–4): 149–163. <https://doi.org/10.1080/15732480701520196>.

- Lam, H. 2017. "Redundancy evaluation of steel-concrete composite twin I-girder bridges." Ph.D. thesis, Dept. of Civil and Environmental Engineering, Waseda Univ.
- Lam, H., W. Lin, and T. Yoda. 2017. "Performance of composite twin I-girder bridges with fatigue-induced cracks." *J. Struct. Eng.* 22 (9): 04017056. [https://doi.org/10.1061/\(ASCE\)BE.1943-5592.0001094](https://doi.org/10.1061/(ASCE)BE.1943-5592.0001094).
- Lin, W., L. J. Butler, M. Z. E. B. Elshafie, and C. R. Middleton. 2019. "Performance assessment of a newly constructed skewed half-through railway bridge through integrated sensing." *J. Bridge Eng.* 24 (1): 04018107. [https://doi.org/10.1061/\(ASCE\)BE.1943-5592.0001334](https://doi.org/10.1061/(ASCE)BE.1943-5592.0001334).
- Lin, W., T. Yoda, Y. Kumagai, and T. Saigyo. 2013. "Numerical study on post-fracture redundancy of the two-girder steel-concrete composite highway bridges." *Int. J. Steel Struct.* 13 (4): 671–681. <https://doi.org/10.1007/s13296-013-4008-8>.
- Lin, W., T. Yoda, N. Taniguchi, H. Kasano, and J. He. 2014. "Mechanical performance of steel-concrete composite beams subjected to a hogging moment." *J. Struct. Eng.* 140 (1): 04013031. [https://doi.org/10.1061/\(ASCE\)ST.1943-541X.0000800](https://doi.org/10.1061/(ASCE)ST.1943-541X.0000800).
- Lin, W., Yoda, T., Taniguchi, N., Lam, H., and Nakabayashi, K. 2016. "Post-fracture redundancy evaluation of a twin box-girder Shinkansen bridge in Japan." In *Proc., IABSE Conf. Guangzhou 2016*. Zürich, Switzerland: International Association for Bridge and Structural Engineering.
- Ma, H., and X. Shi. 2016. "Parametric study on behaviour twin-I girder bridge systems with cross-beams." In *Proc., 2016 Structural Congress (Structures 2016)*. Seoul: Korea Federation of Science and Technology Societies, Jeju Convention Visitors' Bureau, and Korea Tourism Organization.
- Ministry of Construction. 1995. *Standard specifications for steel and composite structures*. Naypyidaw, Myanmar: Ministry of Construction.
- Park, Y., W. Joe, J. Park, M. Hwang, and B. H. Choi. 2012. "An experimental study on after-fracture redundancy of continuous span two-girder bridges." *Int. J. Steel Struct.* 12 (1): 1–13. <https://doi.org/10.1007/s13296-012-1001-6>.
- Samaras, V. A., J. P. Sutton, E. B. Williamson, and K. H. Frank. 2012. "Simplified method for evaluating the redundancy of twin steel box-girder bridges." *J. Bridge Eng.* 17 (3): 470–480. [https://doi.org/10.1061/\(ASCE\)BE.1943-5592.0000280](https://doi.org/10.1061/(ASCE)BE.1943-5592.0000280).
- Sarraf, R. E., D. Iles, A. Momtahan, D. Easey, and S. Hicks. 2013. *Steel-concrete composite bridge design guide*. Research Rep. No. 525. Wellington, New Zealand: New Zealand Transport Agency.
- Tachibana, Y., M. Tsujikado, S. Echigo, S. Takahashi, and C. Miki. 2000. "A study of after-fracture redundancy for two-girder bridges." *J. Jpn. Soc. Civ. Eng.* 2000 (647): 241–251. [https://doi.org/10.2208/jscej.2000.647\\_241](https://doi.org/10.2208/jscej.2000.647_241).
- Takahashi, S., Y. Tachibana, T. Shimura, H. Morishita, H. Ito, and C. Miki. 1997. "Structural details of connection of diaphragm for rationalized plate girder bridges." *J. Jpn. Soc. Civ. Eng.* 1997 (570): 107–118. [https://doi.org/10.2208/jscej.1997.570\\_107](https://doi.org/10.2208/jscej.1997.570_107).
- Yen, J. Y. R., Y. Lin, and M. T. Lai. 1997. "Composite beams subjected to static and fatigue loads." *J. Struct. Eng.* 123 (6): 765–771. [https://doi.org/10.1061/\(ASCE\)0733-9445\(1997\)123:6\(765\)](https://doi.org/10.1061/(ASCE)0733-9445(1997)123:6(765)).